Dalton Transactions

ROYAL SOCIETY OF CHEMISTRY

PAPER

View Article Online
View Journal | View Issue

Cite this: *Dalton Trans.*, 2026, **55**, 4841

Rational development of a drug-delivery device based on MOF UiO-66 for calcium-channel-blocker drugs

Javier Salazar-Muñoz,*[a] Yoan Hidalgo-Rosa,[b] Pia C. Burboa,[c] Cesar Pazo,[a,f] Yazmin Arellano,[a] Camila Le-Roy,[a] Jaime Llanos,[d] Yi-nan Wu,[e] Néstor Escalona,[f] Ximena Zarate[g] and Eduardo Schott*[a]

The administration of drugs with low solubility or absorption, such as the calcium-channel-blocker (CCB) drugs amlodipine, nifedipine, and nimodipine, affects the management of complicated health conditions related to cardiovascular diseases. The development of a drug-delivery device based on MOFs is a rising topic. Thus, in this work, the use of MOF UiO-66 as a platform to develop a drug-delivery device was analyzed using CCB drugs through an empirical and theoretical approach. Our results demonstrate that UiO-66 adsorb and release the three studied drugs without altering the chemical or physical properties of either the material or the drugs. Moreover, computational studies show that dispersive energies are key to the interaction of nimodipine and nifedipine with the material, providing a better understanding of the release behavior observed for each drug. Finally, the effect on the biological activity of the drugs was evaluated using human microvascular endothelial cells, demonstrating that the material can improve the bioavailability of each drug, allowing a 90% reduction in the doses needed to attain a physiological effect. These results support the potential of UiO-66 as a central component in the development of a versatile drug-delivery system aimed at improving the treatment of patients with cardiovascular diseases.

Received 25th August 2025,
Accepted 30th January 2026

DOI: 10.1039/d5dt02037a

rsc.li/dalton

Introduction

Cardiovascular diseases lead to more than 30% of all global deaths. Hypertension is a major risk factor for cardiovascular diseases. It is estimated that 1.28 billion adults worldwide between 30 and 79 years have hypertension.[1] Currently, first-line hypertension drug therapy is based on beta-blockers, angiotensin II receptor blockers, diuretics and calcium-channel-blocker (CCB) drugs. Nifedipine, nimodipine and amlodipine are examples of the first, second and third generation of CCB drugs. They are prescribed to treat different cardiovascular pathologies such as angina pectoris, cerebral vasospasm, subarachnoid hemorrhage, preeclampsia, and hypertension.[2] Nifedipine and nimodipine are both classified as type II biopharmaceutics (BCS type II).[3] This implies that they present high permeability but poor water solubility.[4] Both are considered almost water-insoluble with little variation in their solubility at 37 °C regardless of the pH, whereas amlodipine is classified as a type I biopharmaceutic exhibiting high solubility and permeability.

Nifedipine, nimodipine and amlodipine, also called as Dihydropyridines (DHP), are a class of L-type voltage-gated Ca^{2+} CCBs that are used to lower blood pressure and improve blood flow by relaxing vascular smooth muscle cells (VSMCs).[5,6] However, they can also influence endothelial cells (ECs), the inner layer between blood and tissues. ECs Ca^{2+} depolarization is related to vasodilator signals, such as nitric oxide (NO) and endothelium-dependent hyperpolarization (EDH).[7–9] CCB acts indirectly on ECs to improve vasodilation, mainly by increasing NO production.[10–16] They can also block EC-dependent endothelin-1 production, a vasoconstrictor involved in cerebral vasospasm[17] and inhibit EC apoptosis.[18]

To overcome the limitations related to low solubility and low bioavailability of drugs, different drug-delivery systems (DDSs)

[a]*Departamento de Química Inorgánica, Facultad de Química y de Farmacia, CIEN-UC, CE-UC, Pontificia Universidad Católica de Chile, Santiago, Chile. E-mail: Jsalazarmunoz@gmail.com, maschotte@gmail.com*
[b]*Centro de Nanotecnología Aplicada, Facultad de Ciencias, Ingeniería y Tecnología/ Escuela de Ingeniería del Medio Ambiente y Sustentabilidad, Facultad de Ciencias, Ingeniería y Tecnología, Universidad Mayor, Camino La Pirámide 5750, Huechuraba, Santiago, Chile*
[c]*Department of Pharmacology, Physiology and Neuroscience, Rutgers New Jersey Medical School, Newark, New Jersey, USA*
[d]*Departamento de Química, Facultad de Ciencias, Universidad Católica del Norte, Avda. Angamos 0610, Antofagasta 1270709, Chile*
[e]*College of Environmental Science and Engineering, State Key Laboratory of Pollution Control and Resource Reuse, Tongji University, China*
[f]*Departamento de Química Física, Facultad de Química y Farmacia/Departamento de Ingeniería Química y Bioprocesos, Escuela de Ingeniería, Pontificia Universidad Católica de Chile, Chile*
[g]*Instituto de Ciencias Aplicadas, Theoretical and Computational Chemistry Center, Facultad de Ingeniería, Universidad Autónoma de Chile, Santiago, Chile*

have been developed.[19,20] Nanomaterial-based DDSs are of great interest due to their large surface area and distribution that improve the bioavailability of different compounds. Additionally, nanomaterials trigger enhanced permeation and release effects, which are desirable to improve therapeutic efficiency while lowering side effects. The encapsulation of CCB drugs in nanomaterials has been studied using nanoemulsions containing nimodipine, and these have shown that lipid nanoparticles can improve the plasma availability of the drugs;[21] however, the time permanence of the nanoemulsion in the studied system still needs to be improved. Alawdi *et al.* in 2019[22] reported the use of nanodiamonds to improve the permeation of amlodipine across the blood–brain barrier. Chhabra *et al.* in 2011[23] described how encapsulating amlodipine in a nanoemulsion increases its adsorption in the gastrointestinal tract, thereby increasing its blood concentration. All these efforts have shown that nanomaterials are a good choice for improving CCB performance. However, further studies are needed to enhance the physiological availability of these drugs.

Metal–organic frameworks (MOFs) are coordination polymers that exhibit a great capacity to adsorb different kinds of drugs. Structurally, MOFs can be divided into two main domains, referred to as metallic clusters or secondary binding units (SBUs) with an organic bridging molecule denoted as a linker.[24] MOFs present a three-dimensional array generated by the interconnection of the SBUs by the molecules of the linker. The MOF UiO-66 was first described by Cavka *et al.* in 2008. Its SBUs can be built using Zr, Hf, and Ce using 1,4-benzenedicarboxylic acid.[25] This material has been widely studied over the last decade in different fields due to its physicochemical, thermal, and mechanical stability, high porosity, tunable flexibility, large surface area, and high surface-to-volume ratio.[26–32] Despite their composition, UiO-66 (Zr)-based MOFs are biocompatible materials, and their use as DDSs has been studied for antitumor drugs, antioxidants, and non-steroidal anti-inflammatory drugs.[33–37]

Based on prior studies that show the capability of nanomaterials to enhance the solubility and bioavailability of calcium-channel blockers, this report evaluates, in a pioneering effort, the use of MOF UiO-66 as a key component in the development of a drug-delivery system for CCBs. Thus, through an experimental and theoretical approach, the capacity of UiO-66 to adsorb and release CCBs has been evaluated. Additionally, an *in vitro* calcium-channel blockade assay using human microvascular endothelial cells demonstrated, for the first time, that MOF materials enhance the bioavailability of these drugs, establishing a first step toward the development of a transversal drug-delivery device to improve the quality of life of patients with cardiovascular diseases.

Methodology

Materials

1,4-Benzenedicarboxylic acid (H_2BDC, 98%), zirconium(IV) chloride ($ZrCl_4$, 99%), nifedipine ($C_{17}H_{18}N_2O_6$, N7634), nimodipine ($C_{21}H_{26}N_2O_7$, PHR1293), and phosphate buffered saline pH 7.4 were purchased from Sigma-Aldrich. Amlodipine besylate ($C_{26}H_{31}ClN_2O_8S$, A804204) was purchased from Ambeed. Hydrochloric acid (HCl, 98%), *N*,*N*-dimethylformamide (DMF, 99 wt%), and ethanol (C2H6O, 99.9%) were supplied by Merck.

UiO-66 synthesis

UiO-66 was synthesized as reported by Katz *et al.* in 2006.[26] Briefly, in a 20 mL flask, 0.365 mmol of zirconium tetrachloride ($ZrCl_4$) was dissolved in 4 mL of dimethylformamide (DMF), and 0.6762 mL of concentrated HCl was added as a modulator. The mixture was sonicated for 20 min. Afterwards, 0.507 mmol of 1,4-benzenedicarboxylic acid (BDC), dissolved in 6 mL of DMF, was added to the mixture. This solution was sonicated for another 20 min or until a crystalline mixture was obtained. The resulting mixture was incubated at 80 °C overnight. The solid was collected by centrifugation and washed with two volumes of DMF, followed by two volumes of ethanol. The material was stored in a desiccator until use.

UiO-66(Zr) characterization

The textural properties were determined using a Micromeritics 3Flex instrument from N_2 adsorption–desorption isotherms at −196 °C. Prior to the N_2 adsorption–desorption measurements, the materials were activated for 4 hours at 150 °C using a Micromeritics SmartVac instrument. The surface area was determined using the Brunauer–Emmett–Teller (BET) equation under the Rouquerol criteria,[38] whereas the pore size and the pore volume were determined using the HK and *t*-plot methods, respectively. The thermal stability was determined through thermogravimetric analysis (TGA) and its first derivative (DTG). Samples were measured between 100 °C and 700 °C under N_2 and air atmospheres with a heating rate of 20 °C min^{-1} using a Netzsch STA 449-F5-Jupiter thermobalance. The number of defects in the MOF structure was evaluated by potentiometric acid–base titration.[39] Titrations were carried out using a TitroLine® 7000 automatic titrator from (SI Analytics) with 0.1 M sodium hydroxide. Morphological characterization was performed by scanning electron microscopy (SEM) using a Hitachi Regulus 8100 instrument, and images were analyzed using ImageJ software.[40] Powder X-ray diffraction was measured using a 2nd generation D2 Phaser instrument from Bruker. The crystallite size and crystallinity percentage were calculated using DIFFRAC.EVA® software from Bruker.

Adsorption assay

The adsorption assay was carried out using 5 mg of activated UiO-66(Zr). The drug solutions were prepared by diluting a fresh stock solution of concentration 10 mg mL^{-1} in ultrapure water (mQ) or ethanol. To determine the equilibrium adsorption capacity (Q_e), the material was incubated with 2 mL of drug solution under constant stirring. Samples were incubated for 24 to ensure that the drug concentration reached equilibrium between the solvent and the material. After incubation, each sample was filtered using a 0.2 μm syringe filter. The con-

centration of amlodipine, nifedipine or nimodipine was measured through UV/vis spectrophotometry at 237 nm using a Jasco V-730 instrument. The calculation of Q_e was performed using eqn (1):

$$Q_e = (C_0 - C_e)\frac{V}{m} \quad (1)$$

where Q_e is expressed in mg mg^{-1}, which refers to mg of drug per mg of MOF. C_0 is the initial concentration (mg mL^{-1}) for each of the of NSAIDs, C_e is the concentration of NSAIDs at equilibrium, V is the volume of the assay (mL) and m is the mass of UiO-66(Zr) expressed in mg. Furthermore, to understand the adsorption process and how the solvent affects the adsorption kinetics, the adsorption curves were analyzed using the Langmuir (eqn (2)), Freundlich (eqn (3)) and Temkin (eqn (4)) models.

Langmuir model:

$$Q_e = \frac{Q_m K_L C_e}{(1 + K_L C_e)} \quad (2)$$

Freundlich model:

$$Q_e = K_F {C_e}^{1/n} \quad (3)$$

Temkin:

$$Q_e = B_T \ln(A_T C_e) \quad (4)$$

where Q_e is the quantity of drug adsorbed by the material, Q_m is the maximum adsorption capacity of the material, K_L and K_F are the Langmuir and Freundlich constants, respectively, n is the heterogeneity factor of the Freundlich model, and B_T and A_T are the Temkin constants. For the determination of drug loaded into the material, TGA was used as previously described.[33]

Release assay

The release kinetics were assayed following the model proposed by Wu in 2022.[41] Briefly, 10 mg of loaded UiO-66(Zr) @NSAID was dialyzed against pure water or phosphate buffered saline (PBS) using a Spectra-Por® float-A-Lyzer® dialysis system (1 mL volume, 100 kDa molecular-weight cut-off). At defined time points, the solvent in the secondary container of the dialysis system was replaced with a fresh volume of ultrapure water. The removed solvent was stored at 4 °C until needed for analysis. The concentrations of amlodipine, nifedipine, and nimodipine were determined through UV/vis spectroscopy using Shimadzu's Nexera® HPLC system equipped with a C18 column. The HPLC run program is described in Table 1, where solvent A is methanol, B is acetonitrile, C is water, and D is 5 mM H_2SO_4 in water. The cumulative release curve was analyzed using the equations below.

Zero order:

$$\frac{M_t}{M_\infty} = K_0 \times t \quad (5)$$

First order:

$$\ln\left(1 - \frac{M_t}{M_\infty}\right) = -K_F \times t \quad (6)$$

Higuchi:

$$\frac{M_t}{M_\infty} = K_H \times \sqrt{t} \quad (7)$$

Korsmeyer–Peppas:

$$\frac{M_t}{M_\infty} = K \times t^n \quad (8)$$

where t is the release time, M_t/M_∞ is the drug-release rate at time t with respect to the total amount of drug available in the material, K_0 is the release-kinetic constant of the zero-order model, K_F is release-kinetic constant of the first-order model, K_H is the release-kinetic constant of the Higuchi model, and finally, K is the release-kinetic constant and n is the exponent of release for the Korsmeyer–Peppas model.

Table 1 High-performance liquid chromatography run conditions

Method	Solvent A (%)	Solvent B (%)	Solvent C (%)	Solvent D (%)
Amlodipine	0	75	23	2
Nifedipine	40	60	0	0
Nimodipine	27	35	38	0

Computational methods

Structure optimizations from density functional theory (DFT) methods were carried out using the Amsterdam Density Functional (ADF2023) software package.[42] Relativistic effects play a crucial role in these systems due to the presence of heavy metals like Zr, which strongly influence their chemical and physical behavior.

To accurately capture the electronic structure and properties, these effects should be considered. In this work, the zeroth-order regular approximation (ZORA) method was applied to account for relativistic effects.[43,44] Geometry optimizations were conducted using the generalized gradient approximation (GGA) with the Becke–Perdew (BP86) exchange–correlation functional.[45] All calculations employed a standard Slater-type orbital basis set with two additional polarization functions (STO-TZ2P).[46] The energy decomposition analysis (EDA)[47,48] was performed to explore the interaction energy between the UiO-66(Zr) and the CCB molecule, *i.e.* amlodipine, nifedipine and nimodipine. For the purpose of the EDA, the interacting systems UiO-66(Zr)/CCB were partitioned into two fragments, each representing the interacting part of the system, *i.e.* UiO-66 (Zr) and CCB molecule. The fragmentation was done in such a way that it preserves the symmetry and charge distribution of the individual fragments. This analysis breaks down the interaction energy (ΔE_{Int}) as shown in eqn (9):

$$\Delta E_{Int} = \Delta E_{Pauli} + \Delta E_{Elec} + \Delta E_{Disp} + \Delta E_{Orb} \quad (9)$$

Each term in the energy decomposition analysis was computed as follows. First, the electrostatic energy, ΔE_{Elec}, accounts for the electrostatic interaction between the fragments as they are positioned in the final system. The term, ΔE_{Pauli}, accounts for the repulsive Pauli interaction between occupied orbitals on the two fragments in the interacting system. The dispersion energy term (ΔE_{Disp}) includes the dispersion forces, which act between the fragments introduced *via* Grimme's D3 dispersion correction. Finally, the term ΔE_{Orb} represents potential interactions between molecular orbitals (MOs) associated with charge transfer, polarization, and other related effects. The value of ΔE_{Int} was determined by summing the contributions from each of these components. This decomposition provides insight into the relative importance of each interaction in stabilizing or destabilizing the adsorption of the CCB molecules with the MOFs. To account for the basis set superposition error (BSSE), the interaction energies were corrected using the counterpoise method.[49]

Furthermore, the analysis of orbital contributions was conducted using the Natural Orbital of Chemical Valence (NOCV) method, as introduced by Mitoraj.[50] This approach examines the formation of an interacting system AB (described by the wavefunction ψ_{AB}) from its individual components. Within this framework, the NOCVs identify the channels of charge flow by breaking down the total deformation density, $\Delta\rho$. The NOCV method characterizes these channels of charge flow by expressing them as a series of complementary eigenfunction pairs (ψ_{-k}, ψ_k), associated with eigenvalues ν_k and $-\nu_k$, which have identical magnitude but opposite sign, as depicted in eqn (10):[50]

$$\Delta\rho_{\text{orb}}(r) = \sum_{k=1}^{M/2} \nu_k \left[-\psi_{-k}{}^2(r) + \psi_k{}^2(r)\right] = \sum_{k=1}^{M/2} \Delta\rho_k(r) \qquad (10)$$

The charge-flow pathways between molecular fragments are characterized by these complementary NOCV pairs. By examining NOCV pairs (ψ_{-k}, ψ_k) that share the same eigenvalues of equal magnitude $|\nu_k|$, one can measure the outflow $\Delta\rho_{\text{orb[outflow}(i)]}$ and inflow $\Delta\rho_{\text{orb[inflow}(i)]}$ of electron density within each deformation-density component $\Delta\rho_{\text{orb}}(i)$. These components can be analyzed separately, enabling specific focus on the electron-density outflow and inflow processes associated with each fragment.[51,52]

Biological assays

Trypan blue inclusion assay (cell viability). Human microvascular endothelial cells (HMVEC) (specifically HMVEC-dAd – Human Dermal Microvascular Endothelial Cells, Adult; Lonza, Catalog#: CC-2543) were cultured on glass coverslips in 24-well plates until confluent, then treated for 24 h with either MOF–amlodipine (M1, 260 mg), MOF–nifedipine (M2, 160 mg), MOF–nimodipine (M3, 162 mg), free amlodipine (M4, 176 mg), free nifedipine (M5, 146 mg), free nimodipine (M6, 150 mg), UiO-66(Zr) MOF (M7, 928 mg), or left untreated (control). Post-treatment, cells were washed three times with PBS (3 min each), stained with 0.2% Trypan Blue (1 : 1 in PBS) for 1 min, and fixed with 4% PFA (pH 7.4) for 10 min. Coverslips were rinsed with PBS, dehydrated through graded ethanol (70%, 95%, and 100%), and mounted using ProLong™ Diamond Antifade Mountant (ThermoFisher, Cat #P36965). Images were acquired using a Nikon Eclipse T1 microscope (20× objective). Dead cells were identified by Trypan Blue inclusion and quantified alongside live cells using ImageJ.

Calcium-channel blocker activity. HMVECs were grown to confluence. Cells were left untreated or incubated 2, 6, and 24 hours with M1 (MOF-amlopidine, 260 mg), M2 (MOF-nifedipine, 160 mg), M3 (MOF-nimodipine, 162 mg), M4 (amlodipine, 176 mg), M5 (nifedipine, 146 mg), M6 (nimodipine, 150 mg), or M7 (MOF UiO-66(Zr), 928 mg). After treatment, HMVECs were loaded with 5 μM Fluo-4AM in Tyrode solution containing 5 mM MOPS, with the following composition (mM): 118 NaCl, 5.4 KCl, 2.5 $CaCl_2$, 1.2 KH_2PO_4, 1.2 $MgSO_4$, 23.8 $NaHCO_3$ and 11.1 glucose at pH 7.4, for 30 min. After washing, the cells were transferred to a temperature-controlled imaging chamber maintained at 37 °C on the microscope stage. Basal fluorescence was recorded for 30 s, followed by 2 minutes of stimulation with 1 μM acetylcholine (ACh), an endothelium-dependent vasodilator. A total of 20–30 cells from three coverslips were analyzed. The average value from the three coverslips was used to calculate a single value for each experiment. Variations in fluorescence intensity were expressed as F/F_0, where F represents the fluorescence recorded during the stimulation period and F_0 is the baseline fluorescence value. Fluo-4AM was prepared in dimethyl sulfoxide (DMSO) and diluted to the working concentration in MOPS-buffered Tyrode solution.

Results and discussion

Adsorption assay

The first step toward the implementation of UiO-66 as a drug-delivery device for CCBs is to evaluate the adsorption capacity of the material and determine whether the adsorption of the drug affects the integrity of the material. To understand the adsorption process, the adsorption capacity was evaluated at equilibrium using ethanol as a solvent for the three CCB drugs. This solvent was selected because the three drug compounds are soluble in it and the dispersion of the UiO-66 material is homogeneous. The resulting isotherms were analyzed using standard adsorption models and classified according to the Giles classification system. As can be seen in Fig. S1, the adsorption isotherms obtained for nifedipine and amlodipine resemble the S3-type isotherms, whereas nimodipine exhibits an L3-type isotherm. These isotherms are generated when a reorganization of the adsorbed drugs occurs on the material surface or when a second layer of drug molecules is adsorbed into the material. Additionally, the distinction between L- and S-type curves reflects differences in the interactions between the drugs and the material. In particular, with S-type curves, the initial interaction between the drug and

the material surface is affected by other interactions, such as the interaction with the solvent or adjacent molecules within the same layer. To further evaluate the isotherms, the Langmuir, Freundlich, and Temkin adsorption models were applied. As mentioned before regarding the form of the isotherms, analysis was made by considering the portion of the isotherm up to the first plateau. As observed in Fig. S1, the adsorption capacity of the material does not reach the maximum capacity predicted by the models. As previously described,[33] adsorption of the drugs into the MOF material is governed by their diffusion into the pore structure. This diffusion is affected by the interactions between the drug molecules and the pore walls, the solvent, and adjacent adsorbed molecules. Consequently, the maximum adsorption capacity of the material may not be reached when the drug preferentially remains in the bulk solution rather than entering the pores of the material. Extending the adsorption period beyond 24 hours was not feasible, as preliminary standardization studies showed that the drugs begin to decompose in solution after 24 hours. The instability of these compounds in solution has been previously described, with light identified as one of the main factors increasing their degradation. In considering these restrictions during this work, the maximum incubation time used when combining the material with the drugs was limited to 24 hours, and all the samples were handled and stored in the dark. Moreover, when the theoretical models are considered (Table 2), the best fits for all isotherms corresponded to models describing multilayer adsorption systems, such as the Freundlich and Temkin models. This outcome supports the hypothesis that these drugs interact primarily with the surface of the material.

Table 2 Adsorption parameters obtained for each model used to analyze the adsorption of CCB drugs

	Models parameters		
System	Langmuir	Freundlich	Temkin
UiO66@amlodipine	R^2: 0.958	R^2: 0.969	R^2: 0.941
	K_L: 0.219	K_F: 0.011	$1/B_T$: 1.45×10^{-6}
	Q_{max}: 0.065	n: 1.273	A_T: 13.04
UiO66@nifedipine	R^2: 0.982	R^2: 0.988	R^2: 0.909
	K_L: 0.009	K_F: 0.131	$1/B_T$: 2.32×10^{-5}
	Q_{max}: 13.899	n: 0.912	A_T: 8.637
UiO66@nimodipine	R^2: 0.910	R^2: 0.854	R^2: 0.932
	K_L: 3.552	K_F: 0.029	$1/B_T$: 3.41×10^{-6}
	Q_{max}: 0.032	n: 1.920	A_T: 22.001

Material characterization

Following the adsorption-capacity analysis under the established conditions, we evaluated whether the physical and chemical properties of the material were affected after drug incorporation. For this, the crystallinity, thermal resistance, functional groups, and porosity were assessed before and after drug adsorption.

First, the crystallinity of the material was evaluated through powder X ray diffraction analysis (Fig. 1). Changes to this parameter would reflect that CCB incorporation compromises the structure of the material. As can be observed in Fig. 1 and

Table 3 Analysis of powder X-ray diffraction patterns obtained from the samples

Sample	Crystallite size (Å)	Crystallinity (%)	Size (nm)
UiO-66(Zr)	373.0	92.2	142 ± 17
UiO-66@amlodipine	401.7	77.1	144 ± 24
UiO-66@nifedipine	335.8	87.1	160 ± 28
UiO-66@nimodipine	409.3	89.6	127 ± 23

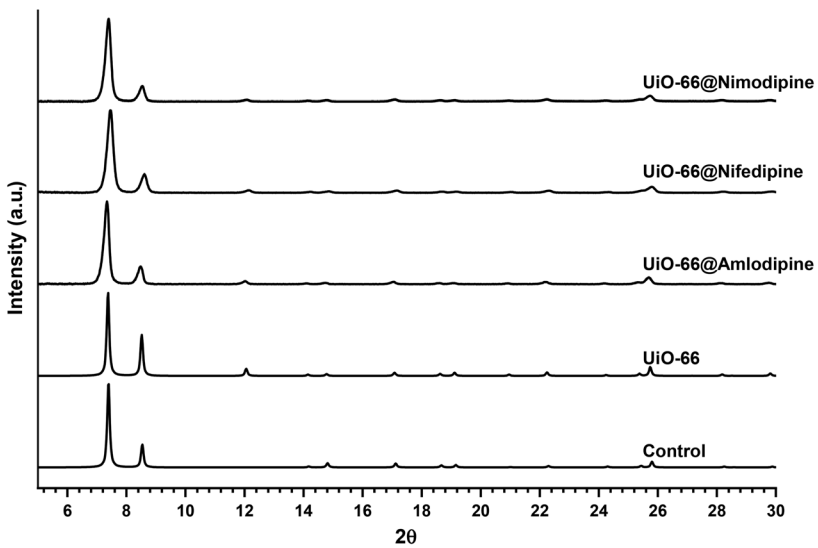

Fig. 1 Powder X-ray diffraction (PXRD) patterns of theoretical crystalline UiO-66 (control), pristine synthesized UiO-66, UiO-66 loaded with amlodipine (UiO-66@amlodipine), UiO-66(Zr) loaded with nifedipine (UiO-66@nifedipine), and UiO-66(Zr) loaded with nimodipine (UiO-66@nimodipine).

Table 3, the structure of the material remains intact after drug adsorption. Considering that the adsorption of the drugs was conducted in ethanol for 24 hours, this result indicates that the incubation of the material with the drugs under these conditions does not affect the structure of the material. These results are in accordance with the previously reported stability of the system exposed to organic solvents such as ethanol.[53] However, the analysis of the crystallite size and the crystallinity percentage, as detailed in Table 3, from each diffraction pattern shows that the loading of the drugs slightly decreases the crystallinity of the material and changes the size of the crystallites (making them, in general, smaller). Considering that crystallite size corresponds to the section of the particle that presents a crystalline array,[54] the results obtained suggest that the incorporation of the drug does not affect the global structure of the material. Additionally, scanning electron microscopy was used to determine the size and morphology of the synthesized material and, as can be seen in Fig. S2, the average crystallite size for each material is around 150 nm. Also, no difference in morphology was observed when amlodipine, nifedipine or nimodipine is loaded into the material, although all materials exhibit a non-defined morphology.

Second, textural analysis of the material (Fig. 2) was evaluated through an N_2 adsorption–desorption assay. The results show that in all cases a type I isotherm model is obtained, which is characteristic of materials with micropores. Additionally, the N_2 adsorption–desorption isotherm of the material slightly decreases when the drug is adsorbed. Table 4 summarizes the apparent surface area (BET surface area) calculated from the adsorption–desorption isotherm together with the pore size and the pore volume. The apparent surface area of the material is larger than that reported experimentally by Katz *et al.*, but it is close to the theoretical surface area that they calculated for this material.[26] For the pristine material, the obtained value of 1739 $m^2\ g^{-1}$ strongly suggests that the material contains defects in its structure. However, the PXRD patterns indicate that these defects do not affect the crystal structure of the material. In considering this observation, the surface area might be larger for two reasons. The first is the washing and activation process used for this material, which involved methanol and dichloromethane followed by activation under dynamic vacuum and heat. This combination improves the desorption of the residual solvent remaining in the pores after synthesis, increasing the availability of empty pore volume in the material.[55,56] A second, and more likely, explanation is the presence of structural defects, specifically missing linkers or clusters.[57] It has been reported that the absence of linkers increases the surface area of this material.[26,58] As shown in Fig. S3, this material exhibits a defect corresponding to 1.55 missing linkers, which implies that from each cluster at least one linker is missing or replaced by the modulator. Similar phenomena were reported by Katz when considering the percentage of linker mass in the TGA experiment, where a loss of 49.5% corresponds to the absence

Table 4 Textural properties for non-loaded and drug-loaded UiO-66 (Zr)

Sample	BET surface area ($m^2\ g^{-1}$)	Pore size (Å)	Pore volume *t*-plot ($cm^3\ g^{-1}$)
UiO-66(Zr)	1739	9.3	0.514
UiO-66@amlodipine	1358	7.4	0.411
UiO-66@nifedipine	1582	7.5	0.437
UiO-66@nimodipine	1593	7.5	0.437

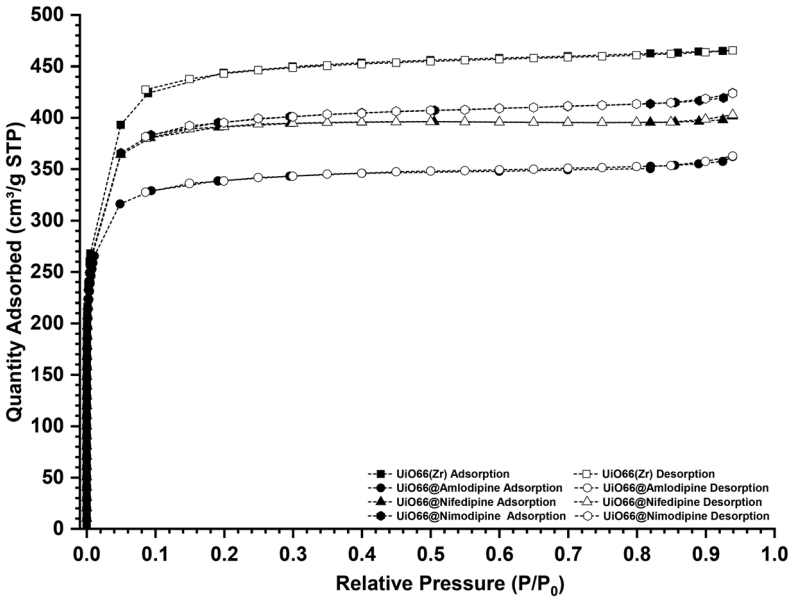

Fig. 2 N_2 adsorption–desorption isotherms for the pristine synthesized material (black squares), loaded with amlodipine (white squares), loaded with nifedipine (black circle)s, and loaded with nimodipine (white circles).

of one linker per cluster. In case of our pristine material, a loss of 46% is observed, which is related to the absence of 1–2 linkers per cluster. Furthermore, when the material is loaded with drugs, the surface area diminishes compared with the untreated material. Also, an isotherm diminution is observed and it can be noted that the pore volume varies in the loaded materials, suggesting that the drugs can penetrate and remain inside the material.

Third, looking to the application of UiO-66 as a DDS for CCBs, how the incorporation of the drug affects the thermal stability of the material was evaluated. It can be observed in Fig. 3 that the incorporation of the drugs does not affect the thermal stability of the material. However, the presence of water adsorbed into the material is increased from 1% in the empty material to 17% in the material loaded with drugs. Moreover, the amount of adsorbed drug can be determined from the thermogram analysis. It should be noted from the thermogram recorded under an N_2 atmosphere that the drug degradation process overlaps with the dihydroxylation of clusters from the material. Thus, it is recommended that such measurements are performed under air. Furthermore, as can be noted from Fig. 3, between 4–5% of the weight loss in the range of 120 °C to 300 °C corresponds to the dihydroxylation. As mentioned, this process can be identified with more clarity when the thermogram is measured under an air atmosphere (Fig. S4), where the presence of the adsorbed drug can be observed and differentiated from the mentioned process. It is important to state that this consideration should be evaluated to avoid an overestimation of the amount of drug loaded into the materials. Taking into account all previous considerations, the amount of drug loaded into the material corresponds to 5%, 5% and 3% for amlodipine, nifedipine and nimodipine, respectively. This observation was consistent when the drug-loading process was repeated using different assays, even when altering the loading conditions with respect to the drug concentration.

Finally, as an important criterion of stability and safety, the chemical characterization of the loaded material was determined through FTIR (Fig. S5). It was observed that there are no changes to the key functional groups present in all the evaluated systems. In accordance with the results obtained from TGA, water is recorded on the spectra as being present in the three drug-loaded materials. Additionally, an increase in the signal in the region of 1000–1100 cm^{-1} was observed, corresponding to the vibration of the C–O bond of the ester and ether groups present in the different drug compounds. Furthermore, characterization using XPS was carried out to determine the stability and composition of the materials before and after loading drugs. As can be noted in Fig. S6, no difference was observed in the XPS spectra for the material before and after loading the MOF with a calcium-channel drug. Additionally, when the Zr region is analyzed, the signals

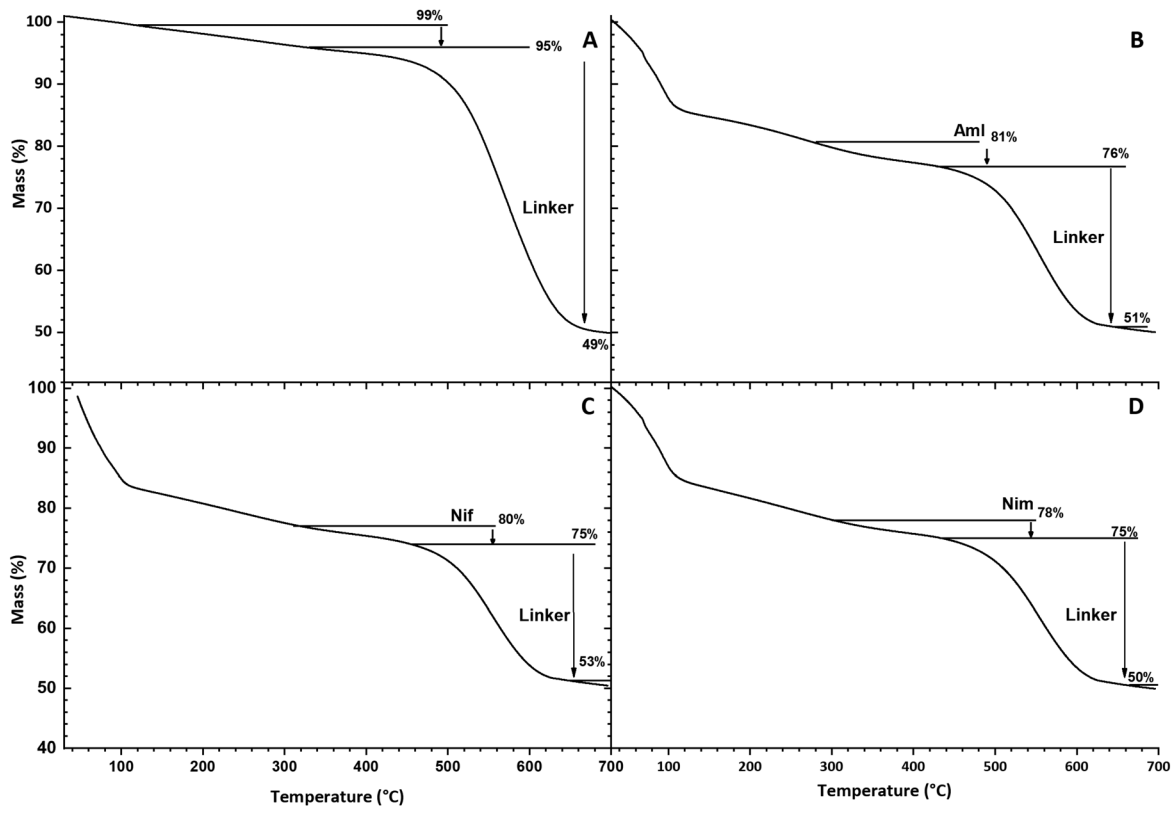

Fig. 3 Thermograms from the thermogravimetric analysis of UiO-66(Zr) as synthesized (A), UiO-66@amlodipine (B), UiO-66@nifedipine (C), and UiO-66@nimodipine (D).

for Zr(IV) remain unchanged, suggesting that the overall process of loading and releasing the drug does not affect the integrity of the material.

To expand the knowledge on the interactions between the material and the different drugs in this study, a series of quantum chemistry calculations was performed. The initial stage of these theoretical investigations involves the structural optimization of the UiO-66(Zr) and the UiO-66(Zr)/CCB interacting systems in their ground electronic states (S_0). In the literature, it is common to encounter research that presents MOFs by either modeling them as large, extended structures or as molecular entities using cluster models. In this context, Hendon *et al.*[59] highlighted cluster models that provide a powerful framework for investigating these materials at higher levels of theory that are often computationally unfeasible when using methods in software suites for materials modeling. In this approach, the cluster model consists of a finite fragment extracted from the extended structure of the MOFs.[33,60,61] Cluster models are ideal for studying localized interactions at specific sites, providing detailed insights with a reduced computational cost. In the current report, the cluster model consists of an explicit node of UiO-66, with the coordination sphere of the metal ions intact. The cluster model employed, $[Zr_6(\mu_3\text{-}O)_4(\mu_3\text{-}OH)_4(BDC)_3(HCOO^-)_8(-OH)(-H_2O)]$, is composed of a node $[Zr_6(\mu_3\text{-}O)_4(\mu_3\text{-}OH)_4(-OH)(-H_2O)]$, with one defect site (hydrated, *i.e.* $(-OH)(-H_2O)$), due to a missing linker (see Fig. 4). Furthermore, in this model, three linkers coordinating to the $[Zr6(\mu_3\text{-}O)_4(\mu_3\text{-}OH)_4]$ remain intact, while eight linkers were shortened to form capping formate groups ($HCOO^-$), as well as $-OH_2$ and –OH groups at the defect sites, which are assumed to arise from missing linkers. This approach allows analysis of the nature and strength of the interactions at the molecular level, focusing on key factors such as interaction energies and binding sites, and can provide a useful insight into drug-release behavior.[62,63] These insights provide a detailed perspective on how the structural and chemical properties of MOFs govern their potential as drug-delivery systems.[33] Fig. S7 in the SI shows the optimized geometries of the UiO-66/amlodipine systems in their ground electronic state (S_0). For this system, the host–guest interaction converges to a configuration in which amlodipine interacts mainly with defect sites of the MOF. Specifically, amlodipine adopts a conformation shifted toward the Brønsted sites of UiO-66, namely the μ_3-OH, $-OH_2$, and –OH protons. As shown in Fig. S7a, hydrogen bonds (HBs) can form between the carbonyl group (>C═O) of the ethyl ester and methyl ester groups of amlodipine, and the –OH and μ_3-OH protons of the UiO-66 SBU, respectively. In particular, the interaction between the methyl ester group of amlodipine and the μ_3-OH protons of UiO-66 is characterized by a calculated bond length of 2 Å and an O–H···O bond angle of 173.5°. Another intermolecular interaction occurs between the carbonyl group (>C═O) of the ethyl ester and the C–H groups of the linker, as well as the –OH groups of UiO-66. This interaction (–OH···C═O) has a calculated bond length of 2.177 Å and an O–H···O bond angle of 142.21°. In the case of the UiO-66@nifedipine system, optimized geometries of the S_0 electronic state are displayed in the Fig. S8a in the SI. In this system, it is possible to observe that the interacting system converged also to the nifedipine interacting with the Brønsted sites of UiO-66 SBU. Specifically, the UiO-66 μ_3-OH protons interact with the methyl ester carbonyl group (–C═O). The calculated bond length of this interaction (μ_3-OH···O═C<) is 1.942 Å, and the bond angle of –O–H···O is 171.9 Å. Finally, for the UiO-66@nimodipine system, the interaction is between the H–O···H–N of the Zr–OH group at the defect site of UiO-66 and the dihydropyridine ring of nimodipine (see Fig. S9a). The calculations reveal that the H–O··· H–N interaction distance is 1.865 Å forming an angle of 155.64°. This final conformation may be attributed to the steric hindrance introduced by the 2-methoxyethoxycarbonyl and isopropoxycarbonyl groups, in comparison with the other studied CCB drugs.

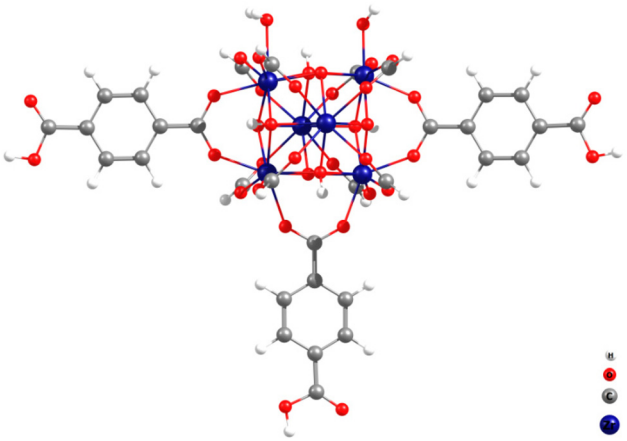

Fig. 4 Cluster model showing an SBU of the UiO-66(Zr) material with one defect, where the white, red, gray and blue spheres represent hydrogen, oxygen, carbon and zirconium(IV) atoms.

Energy decomposition analysis (EDA) was performed to gain deeper insight into the nature of the interaction between UiO-66 and the CCB drugs. As shown in Table 5, the interaction energies indicate only small differences among the studied molecules in terms of total interaction energy. However, the individual energy contributions do vary dramatically.

Only in the UiO-66@amlodipine system is the dispersive component the most important stabilizing term. Thus, the dispersive (van der Waals) forces acting between the UiO-66 and amlodipine play a relevant role in this interacting system. In this case, the dispersion component accounts for 42% of the total stabilizing energy, whereas for UiO-66@nifedipine and UiO-66@nimodipine, ΔE_{Disp} contributes only 29% and 33%, respectively. On the other hand, for UiO-66@nifedipine, the electrostatic component represents 44% of the total attractive energy. In the case of UiO-66@nimodipine, the electrostatic term also makes a large contribution to the total stabilizing energy, accounting for 41% of the stabilizing energy.

Based on the Natural Orbital of Chemical Valence (NOCV) approach proposed by Mitoraj,[64] a detailed analysis of the donor–acceptor interactions between UiO-66 and the CCB drugs was performed. For the UiO-66@amlodipine system, the

Table 5 Morokuma–Ziegler scheme energy decomposition analysis (EDA), values in kcal mol^{-1}, for the UiO-66@DRUGS interacting systems

System	ΔE_{Pauli}	ΔE_{Elec}	ΔE_{Orb}	ΔE_{Disp}	ΔE_{Int}
UiO-66@amlodipine	35.23	−20.77 (35%)	−13.81 (23%)	−24.52 (42%)	−23.87
UiO-66@nifedipine	25.11	−18.82 (44%)	−11.28 (27%)	−12.40 (29%)	−17.39
UiO-66@nimodipine	25.36	−18.25 (41%)	−11.21 (26%)	−12.42 (33%)	−16.53

donor–acceptor interaction is due to intermolecular hydrogen bonding (HB), μ_3-OH···O═C<, formed between UiO-66 and amlodipine. The calculations show that this interaction involves a donation from the oxygen lone pair of amlodipine (from the O═C< group) to the hydrogen atom of the μ_3-OH site in UiO-66. The deformation-density analysis (see Fig. S7b) indicates that this O–H···O interaction corresponds to $\Delta\rho_1$, with an associated orbital-interaction energy of ΔE_{Orb} (1) = −2.99 kcal mol^{-1}, representing 22% to the total orbital-interaction energy (ΔE_{Orb}). Fig. S8b in the SI illustrates the NOCV deformation-density channels for the intermolecular interaction between nifedipine and UiO-66. Based on the result of this interaction, it is observed to be distributed between a donor–acceptor electron lone pair of an oxygen atom (of O═C<) of the CCB drug and the hydrogen atom of the SBU hydroxyl group (μ_3-OH) of UiO-66, thus generating an O···H interaction. The energy corresponding to this deformation-density channel ($\Delta\rho_1$) is ΔE_{Orb} (1) = 5.46 kcal mol^{-1} (see Fig. S8b), which represents 48% of the total orbital-interaction energy (ΔE_{Orb}). According to these results, the HB (μ_3-OH···O═C<) interactions are stronger for the UiO-66@nifedipine system (ΔE_{Orb} (1) = −5.46 kcal mol^{-1} compared with the UiO-66@amlodipine interaction (ΔE_{Orb} (1) = −2.99 kcal mol^{-1}). In the case of the UiO-66@nimodipine system, the deformation-density channels also corroborate the intermolecular HB (H–O···H–N) between UiO-66 and nimodipine (see Fig. S9b). The deformation-density channel ($\Delta\rho_1$) with ΔE_{Orb} (1) = −5.50 kcal mol^{-1} for the S_0 state indicated a HB (O···H) interaction that represents 49% of the total orbital interaction energy (ΔE_{Orb}) for this system.

In summary, EDA-NOCV results showed that the orbital interactions are weaker for the UiO-66@amlodipine system, whereas for the UiO-66@nimodipine and UiO-66@nifedipine systems, the orbital interactions are stronger.

Additionally, the NOCV analysis revealed that the interaction between the CCB drugs and UiO-66 occur through HB at the defect sites of the material. Specifically, deformation density contributions ($\Delta\rho$) indicate that the intermolecular HB involves donor–acceptor interactions between the protons of the μ_3-OH and –OH_2 groups in UiO-66 and the oxygen or hydrogen atoms of the functional groups in the anti-inflammatory molecules. These results further suggest that the intermolecular hydrogen bonding is weaker in the UiO-66@amlodipine system compared to the UiO-66@nifedipine and UiO-66@nimodipine systems.

Release assay

After establishing that the adsorption of the drugs does not affect either the material or the drug, the following analysis was conducted to evaluate whether the material is capable of releasing the adsorbed drug. To test this, the cumulative release of CCB drugs was evaluated when the material is incubated in pH 7.4 PBS buffer at 37 °C emulating the physiological conditions of temperature, acidity, and ionic strength. As observed in Fig. 5, the released amount of adsorbed drug is different for each system. In the case of UiO-66@amlodipine, it can be observed that 80% of the loaded drugs is released from the material after 24 hours of incubation. In contrast, for UiO-66@nifedipine and UiO-66@nimodipine, the cumulative release was 21 and 7.6% of the adsorbed drugs, respectively. The previous energetic interaction analysis can explain this difference in the amounts of drug that are released. Dispersive energies are the main contributor to the interaction between UiO-66 and amlodipine, which could explain the ability of the material to release this molecule into solution, as dispersive energy barriers are easily broken compared to overcoming electrostatic interactions, which require a change to the charge of the system to produce a modification in the interaction between the components of the system. Furthermore, EDA analysis indicates that dispersive forces contribute more to the energy of stabilization. On the other hand, systems based on interaction energy comprising greater electrostatic and orbital energy contributions, as in the case of the UiO-66@nifedipine and UiO-66@nimodipine systems, enable only a low drug-release percentage. This is in addition to the low solubility in the dispersion medium, where both drugs are described as practically insoluble. Despite this, when the cumulative release of the drug in terms of the amount of drug per mL of the system is observed, it is found that the MOF material is capable of releasing 49 μg mL^{-1}, 10 μg mL^{-1} and 0.319 μg mL^{-1} for amlodipine, nifedipine and nimodipine, respectively, during the first hour of incubation. These amounts are sufficient to surpass the recommended plasma concentration of each CCB drug (0.004 μg mL^{-1}, 0.023 μg mL^{-1}, and 0.298 μg mL^{-1} for amlodipine,[65] nifedipine[66] and nimodipine,[67] respectively). As a first step, this amount of drug released is a good indicator of the capacity of the material as a DDS.

To expand the understanding of release kinetics for CCB drug-delivery systems based on UiO-66, the cumulative release of drug for the first 8 hours was analyzed using different theoretical models (Table 6).[68] It was noted that the zero-order model is the one that fits best in order to explain the release process observed for the UiO-66@amlodipine system. This implies that the release of amlodipine from the material depends mainly on the time of incubation. Additionally, the Korsmeyer–Peppas model also showed a good fit for the drug-release curve. however, the n parameter was equal to 1, which

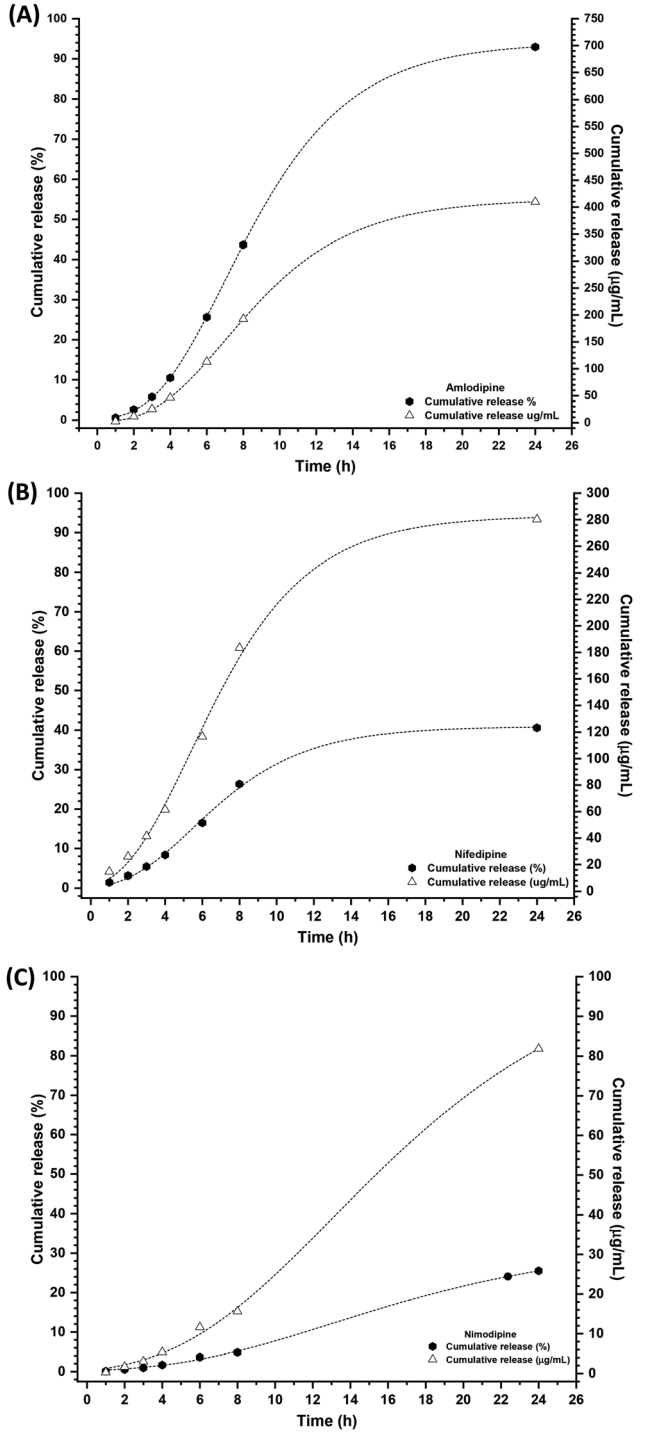

Fig. 5 Cumulative release of CCB drugs: amlodipine (A), nifedipine (B) and nimodipine (C). The black hexagons represent the cumulative percentage release of drug with respect to the amount of drug loaded into the MOF material and white triangles represent the cumulative release of drug in μg mL^{-1}.

means that the release kinetics is equivalent to the zero-order model. In contrast, the Korsmeyer–Peppas model provided the best fit for both of the UiO-66@nifedipine and UiO-66@nimodipine systems, with nifedipine exhibiting a higher release constant than nimodipine, which is consistent with the larger amount released during the analyzed period. When the n parameter in the Korsmeyer–Peppas model exceeds 1, the release process is typically attributed to the swelling of the material and the diffusion of the drugs into the medium. However, in our previous work it was demonstrated that this swelling condition does not affect the integrity of the material, suggesting that diffusion is the main phenomenon affecting the release of the drugs instead of the swelling process. Additionally, it should be noted that the solubility of the drugs released into the solvent is low or practically nil, slowing the release capability of the material.

Table 6 Parameters of the drug-release model applied to analyze the cumulative release of CCB drugs from the UiO-66 MOF material

	Model parameters			
System	Zero order	First order	Higuchi	Korsmeyer–Peppas
UiO66@amlodipine	R^2: 0.998	R^2: 0.968 K_F: 0.084	R^2: 0.775 K_H: 0.145	R^2: 0.999 K: 0.056 n: 1.079
UiO66@nifedipine	R^2: 0.930	R^2: 0.917 K_F: 0.016	R^2: 0.634 K_H: 0.032	R^2:0.979 K: 9.19×10^{-3} n: 1.225
UiO66@nimodipine	R^2: 0.909	R^2: 0.908 K_F: 1.66×10^{-3}	R^2: 0.606 K_H: 3.56×10^{-3}	R^2: 0.989 K: 3.551×10^{-4} n: 1.872

Biological assay

After characterizing the release behavior of the CCB drugs adsorbed into the UiO-66 DDS, and prior to evaluating the calcium influx in a human microvascular endothelium cell line, the cytotoxicity of the systems was assessed (Fig. S10), No evident cytotoxicity was observed when cells were incubated within the different systems.

Although the primary pharmacological effects of CCBs occur in vascular smooth muscle cell, their influence on endothelial-cell calcium responses was also tested, as previous evidence indicates a role for CCBs in EC-dependent Ca^{2+} signalling in the context of cerebral vasospasm. The endothelial-dependent vasodilator acetylcholine (ACh) was used as a positive control for the EC-mediated Ca^{2+} influx. The ability of the UiO-66-based DDS to block the ACH-induced calcium response was then evaluated by incubating the cells with the different systems (Fig. 6). When comparing the Ca^{2+} response, there is no difference between UiO-66@amlodipine (M1) (Fig. 6A) and amlodipine alone (M4) (Fig. 6B), both of which blocked the Ca^{2+} response at similar magnitudes despite the incubation time, which correlates with the observed results in a previous experiment where amlodipine is released following a zero-order model. Cells treated with UiO-66@nifedipine (M2) (Fig. 6C) or treated with nifedipine alone (M5) (Fig. 6D) show a difference between the time needed to block the ACH response, where the M2 system blocked it at all incubation time points, while nifedipine only blocked the response at 6 and 24 hours, but

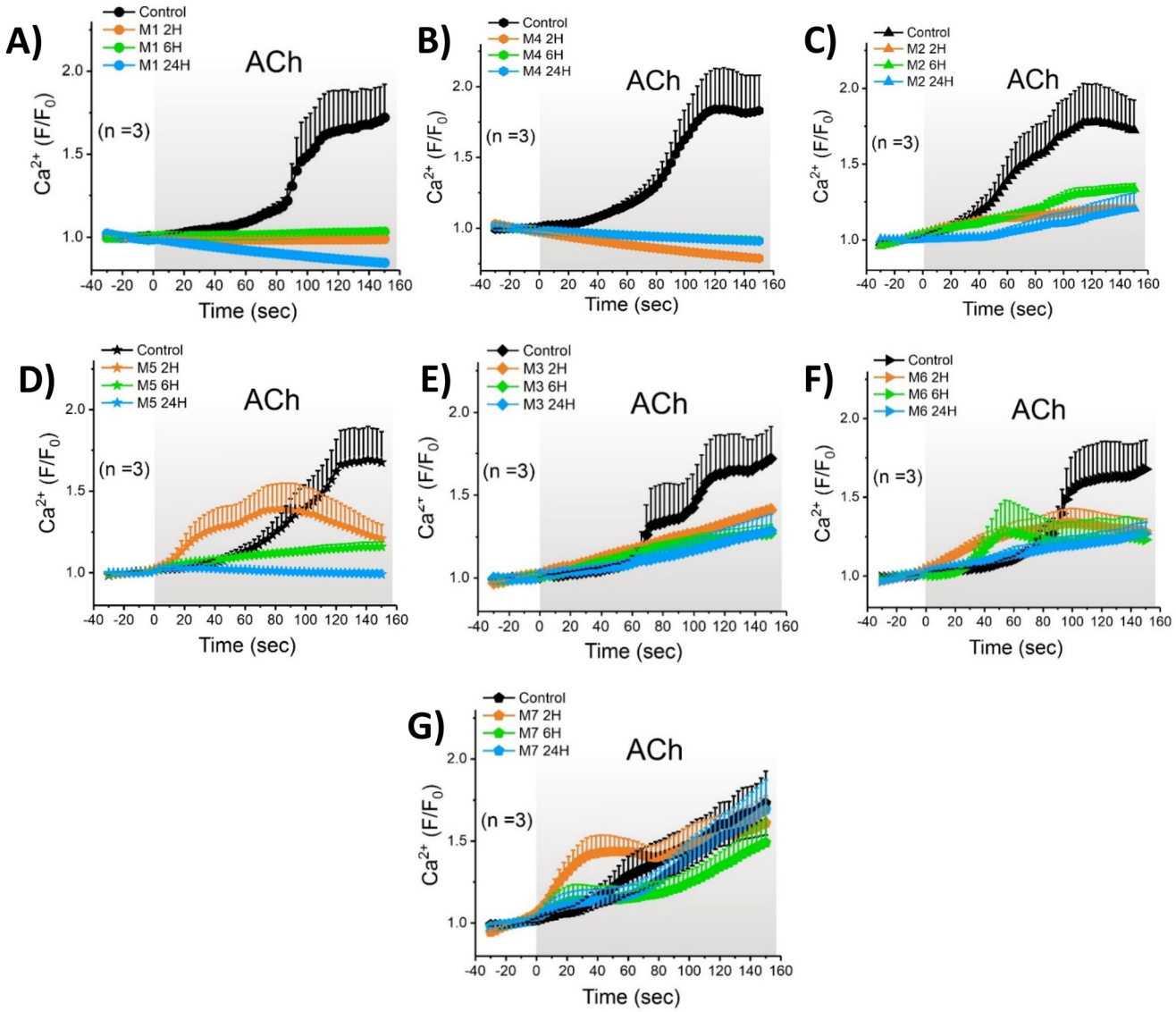

Fig. 6 Endothelial Ca^{2+} response to acetylcholine (ACh) agonist stimulation with Ca^{2+} channel-blocker-carrying UiO-66 MOF. Human microvascular EC (HMVECs) were grown to confluence. HMVECs were left untreated or incubated for 2, 6, and 24 hours with (A) M1 (UiO-66@amlopidine, 260 mg), (B) M2 (UiO-66@nifedipine, 160 mg), (C) M3 (UiO-66@nimodipine, 162 mg), (D) M4 (amlodipine, 176 mg), (E) M5 (nifedipine, 146 mg), (F) M6 (nimodipine, 150 mg) or (G) M7 (MOF UiO-66(Zr), 928 mg). To assess the Ca^{2+} response, cells were loaded with the Ca^{2+} indicator FLUO-4 AM, 30 minutes before incubation ended and stimulated with 1 μM ACh (A to G). Values are mean ± SEM. Control: cells alone.

failed at the incubation time of 2 h. Finally, treatment with UiO-66@nimodipine (M3) (Fig. 6E) shows that the systems have the ability to block the response at all time points, while nimodipine alone (Fig. 6F) failed to block the response at 2 and 6 hours of incubation. Additionally, the treatment of the cells with the untreated system (M7) did not affect the Ca^{2+} measurements (Fig. 6G) or the capacity of the cells to respond to ACH signalling. The lack of effective responses for nifedipine and nimodipine at early time points suggest that the solubility of these drugs is a determining factor in their application. Furthermore, these results demonstrate that the adsorption of the drugs over the material improve the availability and favors the diffusion of the drug into the medium allowing the therapeutic effect to occur earlier when the drug has been administered through a DDS based on the UiO-66 MOF. Moreover, adsorption of the drugs into UiO-66 allows a 90% reduction in the administered dose. This effect is evident when considering the relative amounts of material and drug used in the Ca^{2+} assays (Fig. S11). As shown in this figure, the MOF clearly (with statistical significance) protects the drug and enhances its activity (in every case), thus confirming its role as an effective DDS. Specifically, Fig. S10 (E–G) shows that the activity of the free drug decreases as the exposure time increases. In contrast, when the drugs are incorporated into the MOF, their activity increases, as illustrated in Fig. S10 (A–C).

Conclusion

The application of blood pressure modulators, especially calcium-channel blockers, is a key procedure in treating hypertension-related conditions. The administration of these drugs is challenging due to the solubility and availability of these drugs in the human body. In this work, the potential use of UiO-66(Zr) as a possible alternative to deliver CCB drugs in a sustained manner was evaluated. Our results reinforce the application of this material, demonstrating that it is possible to adsorb the drug over the material and that this process will not affect either the material or the physiological effect of the drugs.

The obtained EDA and NOCV results support the large amount of amlodipine released compared with the amounts of nifedipine and nimodipine, which is also supported by the difference in nature of the intermolecular interactions, particularly hydrogen bonding and dispersive forces, which play critical roles in governing the adsorption and release capabilities of different anti-inflammatory molecules. These findings confirm that variations in both the strength and nature of the interactions directly influence the drug-release behavior, with amlodipine exhibiting stronger dispersive interactions and nifedipine and nimodipine showing interactions with a more pronounced electrostatic character toward UiO-66.

Our biological approach suggests that the application of UiO-66 as a drug-delivery platform for calcium-channel blockers improves the solubility and availability of these drugs, enabling a 90% reduction in the amount of drug needed.

As a future perspective for this work, the application of MOFs as DDSs for CCBs appears highly promising; however, several aspects still require evaluation, including their performance in living organisms and the most appropriate administration route for these materials.

Conflicts of interest

There are no conflicts to declare.

Data availability

Data will be made available on request.

Supplementary information (SI) is available. See DOI: https://doi.org/10.1039/d5dt02037a.

Acknowledgements

The authors thank ANID Chile: FONDECYT 1241917, 1231194, ANID Postdoctoral 3240414, and ANID–Chile, through the Solar Energy Research Center (SERC Chile), under the National Research Centers of National Interest Program, grant CIN250043. This material is based upon work supported by the Air Force Office of Scientific Research under award number FA8655-25-1-8759.

References

1 A. Bathinapatla, S. Kanchi, R. Chokkareddy, R. P. Puthalapattu and M. R. Kumar, Recent trends in the electrochemical sensors on β- and calcium channel blockers for hypertension and angina pectoris: A comprehensive review, *Microchem. J.*, 2023, **192**, 108930, DOI: 10.1016/j.microc.2023.108930.

2 J. Wang, B. F. Palmer, K. Vogel Anderson and P. Sever, Amlodipine in the current management of hypertension, *J. Clin. Hypertens.*, 2023, **25**, 801–807, DOI: 10.1111/jch.14709.

3 A. P. Carlson, D. Hänggi, R. L. Macdonald and C. W. Shuttleworth, Nimodipine Reappraised: An Old Drug With a Future, *Curr Neuropharmacol.*, 2019, **18**, 65–82, DOI: 10.2174/1570159X17666190927113021.

4 L. Z. Benet, The Role of BCS (Biopharmaceutics Classification System) and BDDCS (Biopharmaceutics Drug Disposition Classification System) in Drug Development, *J. Pharm. Sci.*, 2013, **102**, 34–42, DOI: 10.1002/jps.23359.

5 H. Wang, D. Ma, X. Zhu, P. Liu, S. Li, B. Yu and H. Yang, Nimodipine inhibits intestinal and aortic smooth muscle contraction by regulating Ca2+-activated Cl− channels, *Toxicol. Appl. Pharmacol.*, 2021, **421**, 115543, DOI: 10.1016/j.taap.2021.115543.

6 Q. Fang, M. Tian, F. Wang, Z. Zhang, T. Du, W. Wang, Y. Yang, X. Li, G. Chen, L. Xiao, H. Wei, Y. Wang, C. Chen and D. W. Wang, Amlodipine induces vasodilation via Akt2/Sp1−activated miR-21 in smooth muscle cells, *Br. J. Pharmacol.*, 2019, **176**, 2306–2320, DOI: 10.1111/bph.14679.

7 J. Ledoux, M. S. Taylor, A. D. Bonev, R. M. Hannah, V. Solodushko, B. Shui, Y. Tallini, M. I. Kotlikoff and M. T. Nelson, Functional architecture of inositol 1,4,5-trisphosphate signaling in restricted spaces of myoendothelial projections, *Proc. Natl. Acad. Sci. U. S. A.*, 2008, **105**, 9627–9632, DOI: 10.1073/pnas.0801963105.

8 M. A. Lillo, P. S. Gaete, M. Puebla, N. M. Ardiles, I. Poblete, A. Becerra, F. Simon and X. F. Figueroa, Critical contribution of Na^+ –Ca^{2+} exchanger to the Ca^{2+} –mediated vasodilation activated in endothelial cells of resistance arteries, *FASEB J.*, 2018, **32**, 2137–2147, DOI: 10.1096/fj.201700365RR.

9 P. C. Burboa, P. S. Gaete, P. Shu, P. A. Araujo, A. V. Beuve, W. N. Durán, J. E. Contreras and M. A. Lillo, Endothelial TRPV4−Cx43 signalling complex regulates vasomotor tone in resistance arteries, *J. Physiol.*, 2025, JP285194, DOI: 10.1113/JP285194.

10 R. Berkels, D. Taubert, A. Rosenkranz and R. Rösen, Vascular Protective Effects of Dihydropyridine Calcium Antagonists, *Pharmacology*, 2003, **69**, 171–176, DOI: 10.1159/000073659.

11 S. Batova, J. Dewever, T. Godfraind, J. Balligand, C. Dessy and O. Feron, The calcium channel blocker amlodipine promotes the unclamping of eNOS from caveolin in endothelial cells, *Cardiovasc. Res.*, 2006, **71**, 478–485, DOI: 10.1016/j.cardiores.2006.04.013.

12 T. Hayashi, T. Yamaguchi, Y. Sakakibara, K. Taguchi, M. Maeda, M. Kuzuya and Y. Hattori, eNOS-Dependent Antisenscence Effect of a Calcium Channel Blocker in Human Endothelial Cells, *PLoS One*, 2014, **9**, e88391, DOI: 10.1371/journal.pone.0088391.

13 R. P. Mason, R. F. Jacob, J. J. Corbalan, R. Kaliszan and T. Malinski, Amlodipine Increased Endothelial Nitric Oxide and Decreased Nitroxidative Stress Disproportionately to Blood Pressure Changes, *Am. J. Hypertens.*, 2014, **27**, 482–488, DOI: 10.1093/ajh/hpt202.

14 Y. He, D. Si, C. Yang, L. Ni, B. Li, M. Ding and P. Yang, The Effects of Amlodipine and S(-)-Amlodipine on Vascular Endothelial Function in Patients With Hypertension, *Am. J. Hypertens.*, 2014, **27**, 27–31, DOI: 10.1093/ajh/hpt138.

15 T. Maruhashi, M. Kajikawa, S. Kishimoto, S. Matsui, H. Hashimoto, Y. Takaeko, Y. Aibara, F. M. Yusoff, T. Hidaka, K. Chayama, K. Noma, A. Nakashima, C. Goto, Y. Kihara and Y. Higashi, Relationships Between Calcium Channel Blockers and Vascular Function Tests, *Am. J. Hypertens.*, 2019, **32**, 640–648, DOI: 10.1093/ajh/hpz061.

16 C. Peng, L. Yang, C. Zhang, Y. Jiang, L. Shang, J. He, Z. Zhou, X. Tao, L. Tie, A. F. Chen and H. Xie, Low-dose nifedipine rescues impaired endothelial progenitor cell-mediated angiogenesis in diabetic mice, *Acta Pharmacol. Sin.*, 2023, **44**, 44–57, DOI: 10.1038/s41401-022-00948-w.

17 M. A. Yakubu and C. W. Leffler, L-type voltage-dependent Ca^{2+} channels in cerebral microvascular endothelial cells and ET-1 biosynthesis, *Am. J. Physiol.: Cell Physiol.*, 2002, **283**, C1687–C1695, DOI: 10.1152/ajpcell.00071.2002.

18 Y. D. Cho, H. S. Byoun, K. H. Park, Y. I. Won and J. Lim, The Impact of Enteral Nimodipine on Endothelial Cell Apoptosis in an Animal Subarachnoid Hemorrhage Model, *Neurocrit. Care*, 2024, **41**, 608–618, DOI: 10.1007/s12028-024-01980-w.

19 X. Han, J. Chen, Y. Zhao, R. Kang, Y. Wei and S. Zhou, Dual antibody-guided drug delivery systems using MOF-PQDs nanocomposites for precise tumor diagnosis and combination therapy, *Chem. Eng. J.*, 2025, **505**, 159275, DOI: 10.1016/j.cej.2025.159275.

20 Y. Chen, Y. Xu, S. A, B. Shen and S. Zhou, Anti-PD-L1 immobilization on Fe_3O_4 nanocluster-coated AuNR through terpyridine–gadolinium coordination for multimodal imaging and synergistic tumor therapy, *Colloids Surf., B*, 2025, **256**, 115047, DOI: 10.1016/j.colsurfb.2025.115047.

21 S. Huang, Z. Huang, Z. Fu, Y. Shi, Q. Dai, S. Tang, Y. Gu, Y. Xu, J. Chen, X. Wu and F. Ren, A Novel Drug Delivery Carrier Comprised of Nimodipine Drug Solution and a Nanoemulsion: Preparation, Characterization, in vitro, and in vivo Studies, *Int. J. Nanomed.*, 2020, **15**, 1161–1172, DOI: 10.2147/IJN.S226591.

22 S. H. Alawdi, H. Eidi, M. M. Safar and M. A. Abdel-Wahhab, Loading Amlodipine on Diamond Nanoparticles: A Novel Drug Delivery System, *Nanotechnol. Sci. Appl.*, 2020, **12**, 47–53, DOI: 10.2147/NSA.S232517.

23 G. Chhabra, K. Chuttani, A. K. Mishra and K. Pathak, Design and development of nanoemulsion drug delivery system of amlodipine besilate for improvement of oral bioavailability, *Drug Dev. Ind. Pharm.*, 2011, **37**, 907–916, DOI: 10.3109/03639045.2010.550050.

24 K. O. Kirlikovali, S. L. Hanna, F. A. Son and O. K. Farha, Back to the Basics: Developing Advanced Metal–Organic Frameworks Using Fundamental Chemistry Concepts, *ACS Nanosci. Au*, 2023, **3**, 37–45, DOI: 10.1021/acsnanoscienceau.2c00046.

25 J. H. Cavka, S. Jakobsen, U. Olsbye, N. Guillou, C. Lamberti, S. Bordiga and K. P. Lillerud, A New Zirconium Inorganic Building Brick Forming Metal Organic Frameworks with Exceptional Stability, *J. Am. Chem. Soc.*, 2008, **130**, 13850–13851, DOI: 10.1021/ja8057953.

26 M. J. Katz, Z. J. Brown, Y. J. Colón, P. W. Siu, K. A. Scheidt, R. Q. Snurr, J. T. Hupp and O. K. Farha, A facile synthesis of UiO-66, UiO-67 and their derivatives, *Chem. Commun.*, 2013, **49**, 9449, DOI: 10.1039/c3cc46105j.

27 M. Kadhom, M. Al-Furaiji, S. Salih, M. A. Al-Obaidi, G. H. Abdullah and N. Albayati, A review on UiO-66 applications in membrane-based water treatment processes, *J. Water Process Eng.*, 2023, **51**, 103402, DOI: 10.1016/j.jwpe.2022.103402.

28 A. Wang, M. Walden, R. Ettlinger, F. Kiessling, J. J. Gassensmith, T. Lammers, S. Wuttke and Q. Peña, Biomedical Metal–Organic Framework Materials: Perspectives and Challenges, *Adv. Funct. Mater.*, 2024, **34**, 2308589, DOI: 10.1002/adfm.202308589.

29 P. Horcajada, R. Gref, T. Baati, P. K. Allan, G. Maurin, P. Couvreur, G. Férey, R. E. Morris and C. Serre, Metal–Organic Frameworks in Biomedicine, *Chem. Rev.*, 2012, **112**, 1232–1268, DOI: 10.1021/cr200256v.

30 S. Rojas, A. Arenas-Vivo and P. Horcajada, Metal-organic frameworks: A novel platform for combined advanced therapies, *Coord. Chem. Rev.*, 2019, **388**, 202–226, DOI: 10.1016/j.ccr.2019.02.032.

31 I. Abánades Lázaro, X. Chen, M. Ding, A. Eskandari, D. Fairen-Jimenez, M. Giménez-Marqués, R. Gref, W. Lin, T. Luo and R. S. Forgan, Metal–organic frameworks for biological applications, *Nat. Rev. Methods Primers*, 2024, **4**, 42, DOI: 10.1038/s43586-024-00320-8.

32 T. Simon-Yarza, A. Mielcarek, P. Couvreur and C. Serre, Nanoparticles of Metal–Organic Frameworks: On the Road to In Vivo Efficacy in Biomedicine, *Adv. Mater.*, 2018, **30**, 1707365, DOI: 10.1002/adma.201707365.

33 J. Salazar, Y. Hidalgo-Rosa, P. C. Burboa, Y. Wu, N. Escalona, A. Leiva, X. Zarate and E. Schott, UiO-66(Zr) as drug delivery system for non-steroidal anti-inflammatory drugs, *J. Controlled Release*, 2024, **370**, 392–404, DOI: 10.1016/j.jconrel.2024.04.035.

34 Y. Wang, W. Lin, S. Yu, X. Huang, X. Lang, Q. He, L. Gao, H. Zhu and J. Chen, A biocompatible Zr-based metal-organic framework UiO-66-PDC as an oral drug carrier for pH-response release, *J. Solid State Chem.*, 2021, **293**, 121805, DOI: 10.1016/j.jssc.2020.121805.

35 S. Rojas, I. Colinet, D. Cunha, T. Hidalgo, F. Salles, C. Serre, N. Guillou and P. Horcajada, Toward Understanding Drug Incorporation and Delivery from Biocompatible Metal–Organic Frameworks in View of Cutaneous Administration, *ACS Omega*, 2018, **3**, 2994–3003, DOI: 10.1021/acsomega.8b00185.

36 I. Abánades Lázaro and R. S. Forgan, Application of zirconium MOFs in drug delivery and biomedicine, *Coord. Chem. Rev.*, 2019, **380**, 230–259, DOI: 10.1016/j.ccr.2018.09.009.

37 M. Pourmadadi, Z. Omrani, Z. Forootan, M. S. Ebadi and F. Yazdian, UiO-66 nanoparticles as a drug delivery system: A comprehensive review, *J. Drug Delivery Sci. Technol.*, 2023, **86**, 104690, DOI: 10.1016/j.jddst.2023.104690.

38 M. Thommes, K. Kaneko, A. V. Neimark, J. P. Olivier, F. Rodriguez-Reinoso, J. Rouquerol and K. S. W. Sing, Physisorption of gases, with special reference to the evaluation of surface area and pore size distribution (IUPAC Technical Report), *Pure Appl. Chem.*, 2015, **87**, 1051–1069, DOI: 10.1515/pac-2014-1117.

39 R. C. Klet, Y. Liu, T. C. Wang, J. T. Hupp and O. K. Farha, Evaluation of Brønsted acidity and proton topology in Zr- and Hf-based metal–organic frameworks using potentiometric acid–base titration, *J. Mater. Chem. A*, 2016, **4**, 1479–1485, DOI: 10.1039/C5TA07687K.

40 C. A. Schneider, W. S. Rasband and K. W. Eliceiri, NIH Image to ImageJ: 25 years of image analysis, *Nat. Methods*, 2012, **9**, 671–675, DOI: 10.1038/nmeth.2089.

41 C.-J. Wu, Y.-F. Liu, W.-F. Zhang, C. Zhang, G.-B. Chai, Q.-D. Zhang, J. Mao, I. Ahmad, S.-S. Zhang and J.-P. Xie, Encapsulation and controlled release of fragrances from MIL-101(Fe)-based recyclable magnetic nanoporous carbon, *Colloids Surf., A*, 2022, **640**, 128453, DOI: 10.1016/j.colsurfa.2022.128453.

42 D. B. Baerends, E. J. Ziegler, T. Autschbach, J. Bashford, L. A. Bickelhaupt, F. M. Bo, C. Boerrigter, P. M. Cavallo, L. D. P. Chong, *et al.*, ADF2023, SCM, Theoretical Chemistry, Vrije Universiteit, Amsterdam, The Netherlands, 2023, https://www.scm.com.

43 E. Van Lenthe, E. J. Baerends, J. G. Snijders, E. Van Lenthe, E. J. Baerends and J. G. Snijders, Relativistic regular two-component Hamiltonians Relativistic regular two-component Hamiltonians, *J. Chem. Phys.*, 1993, **99**(6), 4597–4610, DOI: 10.1063/1.466059.

44 E. van Lenthe, R. van Leeuwen, E. J. Baerends and J. G. Snijders, Relativistic regular two-component Hamiltonians, *Int. J. Quantum Chem.*, 1996, **57**, 281–293, DOI: 10.1002/(SICI)1097-461X(1996)57:3%253C281::AID-QUA2%253E3.0.CO;2-U.

45 J. P. Perdew and W. Yue, Accurate and simple density functional for the electronic exchange energy: Generalized gradient approximation, *Phys. Rev. B:Condens. Matter Mater. Phys.*, 1986, **33**, 8800–8802, DOI: 10.1103/PhysRevB.33.8800.

46 E. Van Lenthe and E. J. Baerends, Optimized Slater-type basis sets for the elements 1–118, *J. Comput. Chem.*, 2003, **24**, 1142–1156, DOI: 10.1002/jcc.10255.

47 T. Ziegler and A. Rauk, On the calculation of bonding energies by the Hartree Fock Slater method, *Theor. Chim. Acta*, 1977, **46**, 1–10, DOI: 10.1007/bf00551648.

48 K. Kitaura and K. Morokuma, A new energy decomposition scheme for molecular interactions within the Hartree–Fock approximation, *Int. J. Quantum Chem.*, 1976, **10**, 325–340, DOI: 10.1002/qua.560100211.

49 S. F. Boys and F. Bernardi, The calculation of small molecular interactions by the differences of separate total energies. Some procedures with reduced errors, *Mol. Phys.*, 1970, **19**, 553–566, DOI: 10.1080/00268977000101561.

50 M. P. Mitoraj, A. Michalak and T. Ziegler, On the nature of the agostic bond between metal centers and ??-hydrogen atoms in alkyl Complexes. An analysis based on the extended transition state method and the natural orbitals for chemical valence scheme (ETS-NOCV), *Organometallics*, 2009, **28**, 3727–3733, DOI: 10.1021/om900203m.

51 F. Sagan and M. P. Mitoraj, Kinetic and Potential Energy Contributions to a Chemical Bond from the Charge and Energy Decomposition Scheme of Extended Transition State Natural Orbitals for Chemical Valence, *J. Phys. Chem. A*, 2019, **123**, 4616–4622, DOI: 10.1021/acs.jpca.9b01420.

52 K. Devi, S. M. N. V. T. Gorantla and K. C. Mondal, EDA-NOCV analysis of carbene-borylene bonded dinitrogen complexes for deeper bonding insight: A fair comparison with a metal-dinitrogen system, *J. Comput. Chem.*, 2022, **43**, 757–777, DOI: 10.1002/jcc.26832.

53 J. Salazar, Y. Hidalgo-Rosa, P. C. Burboa, Y. Wu, N. Escalona, A. Leiva, X. Zarate and E. Schott, UiO-66(Zr) as drug delivery system for non-steroidal anti-inflammatory drugs, *J. Controlled Release*, 2024, **370**, 392–404, DOI: 10.1016/j.jconrel.2024.04.035.

54 A. Monshi, M. R. Foroughi and M. R. Monshi, Modified Scherrer Equation to Estimate More Accurately Nano-Crystallite Size Using XRD, *World J. Nano Sci. Eng.*, 2012, **02**, 154–160, DOI: 10.4236/wjnse.2012.23020.

55 X. Zhang, Z. Chen, X. Liu, S. L. Hanna, X. Wang, R. Taheri-Ledari, A. Maleki, P. Li and O. K. Farha, A historical overview of the activation and porosity of metal–organic frameworks, *Chem. Soc. Rev.*, 2020, **49**, 7406–7427, DOI: 10.1039/D0CS00997K.

56 N. Al Amery, H. R. Abid, S. Al-Saadi, S. Wang and S. Liu, Facile directions for synthesis, modification and activation of MOFs, *Mater. Today Chem.*, 2020, **17**, 100343, DOI: 10.1016/j.mtchem.2020.100343.

57 G. C. Shearer, S. Chavan, S. Bordiga, S. Svelle, U. Olsbye and K. P. Lillerud, Defect Engineering: Tuning the Porosity and Composition of the Metal–Organic Framework UiO-66 via Modulated Synthesis, *Chem. Mater.*, 2016, **28**, 3749–3761, DOI: 10.1021/acs.chemmater.6b00602.

58 C. V. Mhatre, J. J. Wardzala, M. C. Oliver, M. Islamov, P. Boone, C. Wilmer, L. Huang and J. K. Johnson, The Impact of Missing Linker Defects in UiO-66 on Adsorption and Diffusion of Isopropyl Alcohol, *J. Phys. Chem. C*, 2024, **128**, 13577–13587, DOI: 10.1021/acs.jpcc.4c02982.

59 J. L. Mancuso, A. M. Mroz, K. N. Le and C. H. Hendon, Electronic Structure Modeling of Metal-Organic Frameworks, *Chem. Rev.*, 2020, **120**, 8641–8715, DOI: 10.1021/acs.chemrev.0c00148.

60 X. P. Wu, L. Gagliardi and D. G. Truhlar, Cerium Metal-Organic Framework for Photocatalysis, *J. Am. Chem. Soc.*, 2018, **140**, 7904–7912, DOI: 10.1021/jacs.8b03613.

61 T.-H. T. Le, D. Ferro-Costas, A. Fernández-Ramos and M. A. Ortuño, , Combined DFT and Kinetic Monte Carlo Study of UiO-66 Catalysts for γ-Valerolactone Production, *J. Phys. Chem. C*, 2024, **128**, 1049–1057, DOI: 10.1021/acs.jpcc.3c06053.

62 T. Boroushaki, M. G. Dekamin, S. M. Hashemianzadeh, M. R. Naimi-Jamal and M. Ganjali Koli, A molecular dynamic simulation study of anticancer agents and UiO-66 as a carrier in drug delivery systems, *J. Mol. Graphics Modell.*, 2022, **113**, 108147, DOI: 10.1016/j.jmgm.2022.108147.

63 B. Topuz, H. Kayı, T. Şahin, F.Ş Ersoy, A. Günyaktı and A. Karakeçili, Design of a Zr-based metal-organic framework as an efficient fosfomycin carrier: a combined experimental and DFT study, *New J. Chem.*, 2022, **47**, 1278–1290, DOI: 10.1039/d2nj05100a.

64 M. P. Mitoraj, R. Kurczab, M. Boczar and A. Michalak, Theoretical description of hydrogen bonding in oxalic acid dimer and trimer based on the combined extended-transition-state energy decomposition analysis and natural orbitals for chemical valence (ETS-NOCV), *J. Mol. Modell.*, 2010, **16**, 1789–1795, DOI: 10.1007/s00894-010-0740-6.

65 T. Wang, Y. Wang, S. Lin, L. Fang, S. Lou, D. Zhao, J. Zhu, Q. Yang and Y. Wang, Evaluation of pharmacokinetics and safety with bioequivalence of Amlodipine in healthy Chinese volunteers: Bioequivalence Study Findings, *Clin. Lab. Anal.*, 2020, **34**, e23228, DOI: 10.1002/jcla.23228.

66 H. Zhang, S. Wang, H. Wang, T. Zhi, J. Ren, Y. Wang, Z. Yao, P. Zhang, N. Ye and R. Zhang, Comparative Bioequivalence and Food Effect of Two Formulations of 30–mg Nifedipine Controlled–Release Tablets in Healthy Chinese Adults, *Clin. Pharmacol. Drug Dev.*, 2024, **13**, 499–505, DOI: 10.1002/cpdd.1396.

67 M. M. Moser, K. Rössler, D. Hirschmann, L. Gramss, A. Tahir, W. Plöchl, J. Herta, A. Reinprecht, M. Zeitlinger and A. Hosmann, Cerebral Ischemia Protection After Aneurysmal Subarachnoid Hemorrhage: CSF Nimodipine Levels After Intravenous Versus Oral Nimodipine Administration, *Clin. Pharmacol. Ther.*, 2025, **117**, 589–597, DOI: 10.1002/cpt.3499.

68 M. L. Bruschi, Mathematical models of drug release, in *Strategies to Modify the Drug Release from Pharmaceutical Systems*, Elsevier, 2015, pp. 63–86. DOI: 10.1016/B978-0-08-100092-2.00005-9.